Observations on the Drag of Conical Bodies at Transonic Speeds

R. F. Starr* and M. O. Varner†
ARO, Inc., Arnold Air Force Station, Tenn.

A study of the drag variation of conical bodies at transonic speeds in a wind tunnel and aeroballistic range has yielded some insight into wall interference phenomena and sting effects. The drag reduction of these conical bodies, caused by wall interference near Mach 1, is similar to those severe trends previously observed on longer slender bodies of revolution. However, a transonic test section wall which can be reduced in porosity near Mach 1 (variable porosity with Mach number) appears to measurably reduce the wall interference problem.

The influence of a sting on the base drag of these bodies has been demonstrated to be important, about 5 to 10%, and a sophisticated mathematical model of the transonic base flowfield has been developed. This model treats the base drag for various forebody cone angles and is valid for stings up to one half the body diameter in size.

Nomenclature

A = body cross-sectional area
A_B = body base area
A_{DS} = flow area defined by intersection of dividing streamline and oblique shock (see Fig. 8)
a = constant as defined in Eq. (4)
a_∞ = freestream speed of sound
C_D = local drag coefficient
C_{DB} = base drag coefficient
C_{DF} = forebody drag coefficient
C_{D_0} = drag coefficient at zero angle of attack
C_p = pressure coefficient
C_{ζ} = Crocco number as defined in Ref. 11 based on free-streamline Mach number
dB, dn, ds = base, nose, and sting diameter, respectively
G_B = base bleed flow rate as defined in Eq. (10)
H = bleed number equal to $G_B/(\rho_\zeta a_\infty A_{DS})$
I_1 = integral function as defined in Ref. 11 where $I_1 = I_1(C_\zeta, \eta)$
K_{DS} = base backflow coefficient
k_0 = constant as defined in Eq. (5)
M_ζ = local free streamline Mach number
M_∞ = freestream Mach number
R = free streamline radius as function of x
Re = Reynolds number
Re_D = Reynolds number based on base diameter
r_B = base radius
r_{DS} = radius of dividing streamline at oblique shock
r_s = sting radius
r_{sh} = shock radius as depicted in Fig. 6
t = time
u_ζ = local free streamline velocity
X = tangent reference coordinate relative to the free streamline as defined in Eq. (9)
x = longitudinal coordinate or intrinsic coordinate as defined in Eq. (9)
x_{sh} = longitudinal shock position as depicted in Fig. 6
Y = normal reference coordinate relative to the free streamline as defined in Eq. (9)
y = intrinsic coordinate as given in Eq. (9)
α = shock angle relative to the free streamline
γ = specific heat ratio
δ_B = shoulder cone angle
ζ = local slope of free streamline, a function of x
ζ_{DS} = slope of dividing streamline at shock intersection (see Fig. 8)
ζ_{sH} = slope of free streamline at shock intersection (see Fig. 7)
η = similarity variable for mixing layer as defined in Eq. (8)
η_j = similarity variable defining zero base bleed flow rate
η_m = displacement of the intrinsic system with respect to the reference system as given in Eq. (9)
η_s = similarity variable defining a base bleed flow rate of G_B
ν = variable of integration
ρ = freestream density
ρ_ζ = local density on the free streamline
σ = jet spread parameter as defined in Ref. 10
Φ = velocity potential of the mixing layer as defined in Eq. (8)
ϕ = perturbation velocity potential
ψ = a function as defined in Eq. (6).
ω = $C_{DB} - \zeta^2$

Presented as Paper 76-90 at the AIAA 14th Aerospace Sciences Meeting, Washington, D.C., Jan. 26-28, 1976; submitted March 15, 1976; revision received July 19, 1976. The research reported herein was conducted by the Arnold Engineering Development Center (AEDC), Air Force Systems Command (AFSC). Research results were obtained by personnel of ARO, Inc., contract operator at AEDC. Further reproduction is authorized to satisfy needs of the U.S. Government.

Index category: Subsonic and Transonic Flow.

*Research Engineer, Propulsion Wind Tunnel Facility. Member AIAA.

†Research Engineer, von Kármán Gas Dynamics Facility. Member AIAA.

Introduction

THE magnitude and variation of aerodynamic coefficients measured on models in transonic wind tunnels near Mach 1 have come under increased scrutiny in the past few years. Wall-interference-dominated problems have been demonstrated on two-dimensional airfoils and three-dimensional wings for cases of supercritical flow and on bodies of revolution near the drag divergence Mach number. The magnitude of the wall interference on the measured aerodynamic parameters can be significant. Mislocation of the shock terminating the supercritical flow region on an airfoil by as much as 10-20% of the chord and a complete alteration of the attached-separated flow picture over the

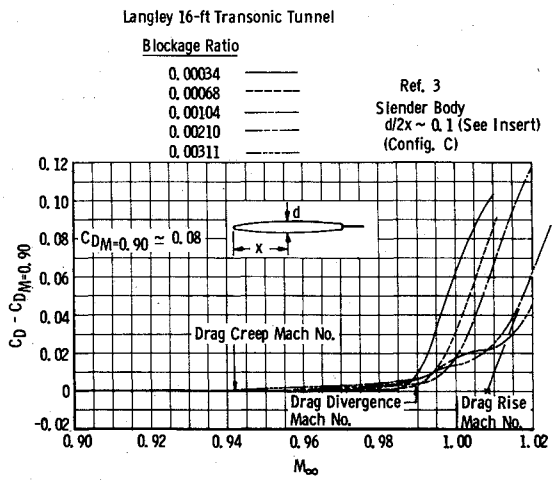

Fig. 1 Drag variation on slender bodies of revolution near Mach 1 for several blockage ratios (fixed-open-area, slotted-wall).

trailing edge of the airfoil are not uncommon.[1,2] In addition, the measured drag at Mach 1 may be reduced to nearly one-half its true value by a very modest solid blockage for slender bodies of revolution.[3]

The influence of solid blockage on the drag of a slender body, as measured in a fixed-open-area, slotted-wall wind tunnel, is given in Fig. 1.[3] It can be seen that even the very modest blockage ratios of the referenced experiments have a pronounced effect on the drag variation near Mach 1. A "drag creep Mach number," which is noted in Fig. 1 for the largest blockage case, and a "drag divergence Mach number," which is also noted in Fig. 1 for one blockage condition, are parameters used by Couch[3] to quantify wall interference phenomena. A "drag rise Mach number," defined as the intersection of the maximum slope tangent to the drag curve with the subsonic drag value, and simply the absolute drag at Mach 1 are also useful parameters for assessing blockage effects (see Fig. 1). Data obtained on 12-1/2 deg semiangle cones[4] also demonstrate a strong effect of blockage on the drag near Mach 1.

The primary purpose of the study described in this paper is to examine the effects of model support and wall interference on the drag of a conical body in the transonic speed range. This involves an assessment of the drag divergence Mach number, drag rise approaching Mach 1, and drag peak between Mach 1 and 1.1 under the condition of negligible wall interference and in the absence of sting effects. Experiments have been conducted in the 10 ft diam AEDC Hyperballistic Range (G) and in the AEDC 4 ft transonic Aerodynamic Wind Tunnel (4T). Since the base drag has a dominant influence on the transonic drag variation for a slender, blunt-based body, a theoretical analysis of the base flowfield has also been completed. The purposes of the analysis are to 1) provide a mathematical model for the transonic base flow problem, 2) define analytically the effects of the presence of a sting on base drag in the transonic speed range for axisymmetric bodies, and 3) allow for the quantitative separation of blockage and sting effects in base drag obtained from existing transonic wind tunnels. The present base drag analysis differs significantly from previous methods in that the present analysis incorporates 1) a base bleed flow from the wake into the dead-air region behind the body which is not included in other models, and 2) a simple, inviscid, free-streamline solution valid in the transonic region. Refined base drag data which will be presented, supplemented by detailed photographs of the wake flow region, give confirmation to the validity of the present base drag model.

As a result of this combined experimental and theoretical study, some observations on the relative blockage effects in solid wall, fixed-open-area-wall, and variable-open-area-wall transonic tunnels can be made. Also the influence of a sting

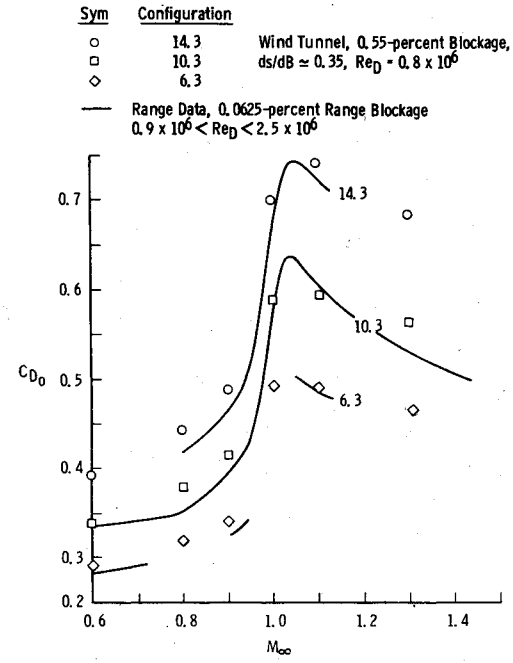

Fig. 2 Drag variation at transonic speeds for a family of cones.

on the drag at transonic speeds will be quantified for these conical bodies.

Models and Test Conditions

The models tested in this study were spherically blunted cones of 6, 10, and 14 deg half-angles. The models tested in the wind tunnel had open bases, that is, the conical skirt was not closed at the base, and the sting was attached near the nose of the body. The base diameter of these models was 4 in., corresponding to a 0.0055 tunnel solid blockage ratio. The models used in the range tests were primarily closed base; however, two shots were made with open-base models. The range models were 1.9, 3, and 6 in. in diameter, resulting in solid blockage ratios of 0.00025, 0.000625, and 0.0025, respectively. The various configurations will be identified in the following manner:

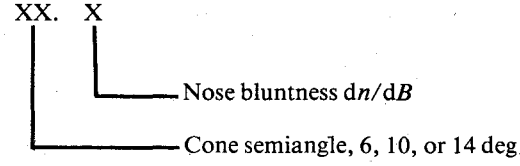

Flights were made in Range G from Mach 0.5 to 1.5 with primary emphasis on the drag rise region between Mach 0.90 and 1.1. All range flights were made at atmospheric pressure (Re/ft $\simeq 5$ to 8×10^6 for $0.8<M_\infty<1.2$) with the corresponding base diameter Reynolds number, Re_D, varying between the limits of 0.8×10^6 and 4×10^6. Visual studies of schlieren photographs taken during the range tests indicated fully developed turbulent flow at the cone shoulder for all models and conditions tested. The weight of the models was selected such that the model decelerated about 10-15% in Mach number during each flight. Thus nearly continuous drag data were obtained over a 0.1 to 0.15 Mach increment on each flight, and the launch velocities were tailored to obtain overlapping data over several flights.

The wind tunnel data were obtained at discrete Mach numbers of 0.6, 0.8, 0.9, 1.0, 1.1, and 1.3 and primarily at an Re/ft of 2.5×10^6. The sting diameter was about 0.35 of the model base diameter and of constant diameter for more than three base diameters downstream. Variation of Re_D from 0.83 to 1.75×10^6 revealed no Reynolds number effect on the axial-force or wind tunnel base drag coefficient. In addition,

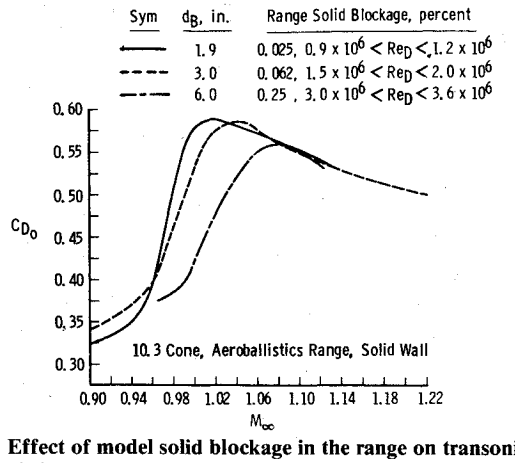

Fig. 3 Effect of model solid blockage in the range on transonic drag characteristics.

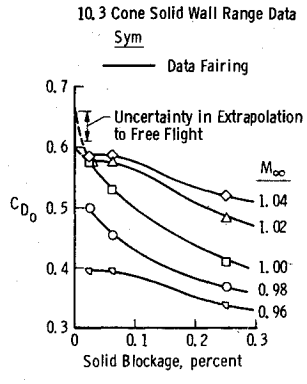

Fig. 4 Effect of range solid blockage on drag coefficient at specific Mach numbers.

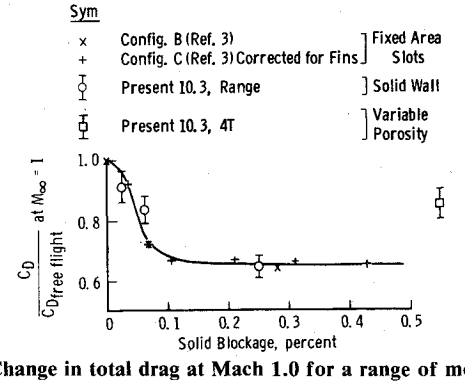

Fig. 5 Change in total drag at Mach 1.0 for a range of model solid blockage.

the overlapping of Re_D for the range and wind tunnel tests substantiates the observation that the flow over the cone shoulder was essentially fully developed and turbulent for all conditions compared.

Standard techniques were used to reduce the range and wind tunnel data. Precision of the drag coefficient data for the range test was ±1.5% and for the wind tunnel varied from ±0.4% at Mach numbers below 1.1 to ±1.0% at Mach 1.3.

Experimental Results

Drag Data

The variation of the drag coefficient with Mach number at transonic speeds is given in Fig. 2 for the 6.3, 10.3, and 14.3 cones. The aeroballistics range data are shown by curves which represent the mean of the experimental results. The range data were obtained at a model base area to range cross-sectional area ratio of 0.0625%. In the range, the definition of solid blockage as defined for wind tunnels is not strictly valid. For comparative purposes, however, the flow distortion effect on the model in the wind tunnel and in the range are assumed equivalent for equal values of wind tunnel solid blockage and the ratio of model base area to range cross-sectional area (range blockage). Although the data obtained on the 6 and 14 deg configurations are limited, sufficient 10 deg data were obtained to establish a drag creep Mach number at about 0.78 and a drag divergence Mach number at about 0.95. Data from the 4 ft transonic facility are also given in Fig. 2 for specific Mach numbers. The solid blockage in the wind tunnel was 0.55%. No measurable differences were detected in the range measurements of drag for open- and closed-base configurations between Mach 1.0 and 1.3. Hence, the differences between the range and wind tunnel data, which are generally about 2-10% in drag coefficient, can be attributed to wall interference effects coupled with sting effects, assuming that the effects attributable to slight Re/ft and Re_D mismatches are negligible. Generally speaking, the data differences below about Mach 0.9 and above Mach 1.1 can be attributed largely to sting effects, whereas the data differences between those Mach number limits are most probably attributable to wall interference, partially offset by sting effects. These two discrepancies will be quantified in the following sections.

Wall Interference

Three 10.3 cones of different sizes were tested in the aeroballistics range to confirm wall interference trends at transonic speeds. The result of the wall interference investigation is given in Fig. 3. As the model size is increased, the drag creep occurs earlier, as evidenced by the data at Mach 0.9, and the drag rise is delayed, as evidenced by the data at Mach 1.0. The drag above about Mach 1.06 is largely unaffected by range blockage variations up to 0.25%. The range, of course, has a solid wall. These trends observed on relatively short conical bodies are in excellent agreement with the results for a much longer slender body given in Ref. 3, as can be seen by referring to Fig. 1. These trends with model size are displayed in Fig. 4 in a slightly different fashion. Note that below about Mach 0.96 and above Mach 1.04 the influence of model size is reduced when compared to its effect between these two limits. Since the model flowfield was fully turbulent for all model sizes and Mach numbers tested, the effect of Re_D mismatch on the trends of C_{D_0} associated with model size (range blockage) was assumed negligible.

The interesting point is that when the drag at Mach 1.0 is viewed as a percentage change from a free-flight value, these data and the results of Ref. 3 collapse to an almost identical curve, as shown in Fig. 5. The bands shown on the present results represent the uncertainty in extrapolation to free flight (see Fig. 4). As the model size is increased, the percentage reduction in the total drag at Mach 1.0 can be as high as 30-40% for both categories of bodies. One additional observation is that the fixed-open-area wall does not really alleviate wall interference phenomena right at Mach 1.0 any better than the solid wall.[3] Most of the recent results utilizing a variable-porosity wall demonstrate that the porosity required to minimize wall interference at Mach 1.0 is significantly different from that required at the subsonic or the higher supersonic speeds (1.1 to 1.3).[5] Hence the fact that a wall whose open area is fixed for good flow at subsonic speeds does not alleviate interference at near Mach 1.0 is not surprising.

The present results from the variable-porosity Tunnel 4T are also given in Fig. 5. In spite of the comparatively high blockage, these drag data are not nearly as affected at Mach 1.0 as the fixed-open-area or solid-wall results. The porosity utilized during this test at Mach 1.0 (1.5%) was established from the results of testing a cone-cylinder model and minimizing the average of the pressure disturbances reflected from the wall.[5] It is possible that a slight additional adjustment in porosity, beyond the sensitivity of the cone-

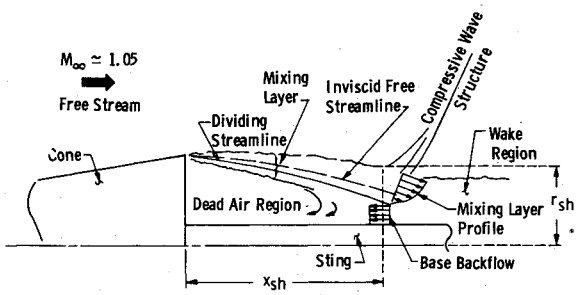

Fig. 6 Typical base flow region for a cone-sting configuration showing parameters of importance.

cylinder technique, could further improve attenuation of wall interference effects at Mach 1.0 and further improve the drag even at this higher blockage. Some recent data on a small winged body[2] indicate that no distinguishable wall interference phenomena could be detected in the variable-porosity tunnel for solid blockage of 0.25% at $M_\infty = 1.0$. This observation is in good qualitative agreement with Fig. 5 and indicates that the variable-porosity tunnel might be good for model blockages of 10-20 times the fixed-wall tunnels or solid-wall range at Mach 1.0.

If one wishes to utilize the data given in Fig. 2 in the absolute sense, it should be emphasized that, based on Fig. 4, the drag at Mach 1.0 is probably about 15% too low, with the error decreasing to near zero at Mach 0.96 and 1.02.

Mathematical Base Drag Model

The calculation of base drag for both two-dimensional and axisymmetric bodies has received continued study over the past twenty years. A review of base drag estimation techniques through 1965 is given in Ref. 6.

Since the base drag contribution of a blunt-based conical body may be a significant portion of the total drag, the need for a model describing the flow process in the base region of axisymmetric bodies at transonic speeds is evident. Thus, an analysis is presented that predicts the effects of the sting, base cone angle, and freestream Mach number on base drag. Figure 6 displays the interacting parameters to be employed in the base pressure model. The inviscid analysis which defines the free-streamline solution and the compressive wave structure region is based on the axisymmetric transonic perturbation theory of Tani[7] as extended by Aoyama.[8] The two-dimensional theory of Korst[9] is used to define the mixing-layer region. A closure criterion is proposed that allows for a base backflow (see Fig. 6) and includes the effects of the sting on the resulting base pressure.

Consider the coordinate system, body, and flow geometry as shown in Fig. 7. From Aoyama,[8] the free-streamline shape in transonic flow is governed by Eq. (1), where ϕ is the perturbation velocity potential, M_∞ is the freestream Mach number, and R is the free-streamline radius as a function of x.

$$\frac{dR}{dx} = -\frac{2}{5}\phi - \frac{2}{3}\sqrt{(\gamma+1)M_\infty^{2/3}}\left[\frac{d\phi}{dx} + \frac{M_\infty^2 - 1}{(1+\gamma)M_\infty^2}\right]^{3/2} \tag{1}$$

The pressure coefficient C_p along the free streamline is given by

$$C_p = -2\frac{d\phi}{dx} - \left(\frac{dR}{dx}\right)^2 \tag{2}$$

Equation (1) is strictly valid only as R approaches r_B, the base radius.[7] However, good agreement between theory and experiment for boattail afterbodies[8] suggests that Eq. (1) may be used for values of R somewhat different from r_B. Assuming that the pressure coefficient in the dead-air region is constant and equal to $-C_{DB}$, where C_{DB} is the base drag coefficient, Eqs. (1) and (2) may be combined to form the

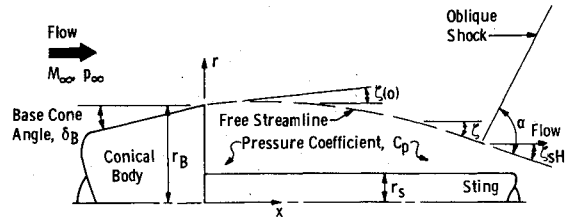

Fig. 7 Flow and body geometry for inviscid analysis.

governing equation for the free-streamline shape, Eq. (3), as a function of C_{DB}.

$$\frac{d\zeta}{dx}\left\{1 - a\zeta\left[k_0 + \frac{C_{DB}}{2} - \frac{\zeta^2}{2}\right]^{1/2}\right\} = \frac{1}{5}(\zeta^2 - C_{DB}) \tag{3}$$

Here, ζ is the free-streamline slope where $\zeta \simeq dR/dx$, and a and k_0 are constants given by

$$a \equiv \sqrt{(1+\gamma)M_\infty^{2/3}} \tag{4}$$

$$k_0 \equiv \frac{M_\infty^2 - 1}{(1+\gamma)M_\infty^2} \tag{5}$$

Equation (3) is directly integrable, leading to an implicit relationship for $\zeta(x)$.

$$x + \text{constant} = -\frac{5}{2C_{DB}^{1/2}}\ln\left[\frac{\zeta + C_{DB}^{1/2}}{|\zeta - C_{DB}^{1/2}|}\right]$$

$$-\frac{5a}{\sqrt{2}}(2k_0+\omega)^{1/2} - \frac{5a\,k_0}{\sqrt{2}}\psi(\zeta;\, C_{DB}, M_\infty, \gamma) \tag{6}$$

where

$$\psi(\zeta; C_{DB}, M_\infty, \gamma) \equiv \begin{cases} \dfrac{1}{\sqrt{2k_0}}\ln\left[\dfrac{(2k_0+\omega)^{1/2} - \sqrt{2k_0}}{(2k_0+\omega)^{1/2} + \sqrt{2k_0}}\right], & M_\infty > 1 \\ -2/\omega^{1/2}, & M_\infty = 1 \\ \dfrac{2}{\sqrt{-2k_0}}\tan^{-1}\sqrt{\dfrac{(2k_0+\omega)}{-2k_0}}, & M_\infty < 1 \end{cases}$$

and $\omega \equiv C_{DB} - \zeta^2$. The constant of integration is evaluated at $x=0$, where it is assumed that the flow at the cone shoulder is sonic.[8] Thus

$$\left[\frac{3}{2M_\infty\sqrt{1+\gamma}}\right]^{2/3}\left[\delta_B - \zeta(o)\right]^{2/3} + \frac{\zeta^2(o)}{2} = k_0 + \frac{C_{DB}}{2} \tag{7}$$

where δ_B is the shoulder cone angle (see Fig. 7). For cases where the flow at the cone shoulder is greater than Mach 1, Eq. (7) is replaced by a Prandtl-Meyer expansion. Equation (6) coupled with the boundary condition, Eq. (7), gives the free-streamline shape as a function of x for a known value of C_{DB}.

Employing the exact shock relations, an oblique shock is assumed to turn the free-streamline flow back parallel with the main stream flow and return the local pressure to freestream conditions. Equations (6) and (7) and the oblique shock relations give the inviscid solution for the free-streamline flow region behind the body as a function of the base drag coefficient leading to an infinite number of possible solutions.

In order to produce a unique solution for the base drag problem, the mixing-layer theory of Korst[9] will be applied to the inviscid problem. For simplicity, it is assumed that the ef-

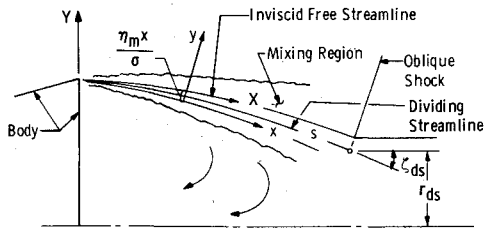

Fig. 8 Coordinate system and flow geometry of mixing region.

fects of Reynolds number and boundary-layer character at the cone shoulder are small and, thus, are neglected. Since the mixing layer is thin relative to the free-streamline geometry, the two-dimensional mixing theory is applied locally to the axisymmetric base flow region. From Korst,[9] the velocity ratio Φ for fully developed isoenergetic turbulent jet mixing is

$$\Phi = 1/2(1+\text{erf}\ \eta) \tag{8}$$

where

$$\Phi = u/u_\zeta$$

$$\text{erf}\ \eta = \frac{2}{\sqrt{\pi}}\int_0^\eta e^{-\nu^2}\,d\nu$$

and

$$\eta = \sigma y/x$$

Here, u_ζ is the free-streamline velocity, u is the x-component of velocity in the mixing region, and $\sigma = \sigma(M_\zeta)$ is the jet spread parameter assuming a fully developed turbulent mixing layer.[10] The intrinsic coordinates x and y are displayed from the reference system (X, Y) measured with respect to the free streamline such that

$$Y = y - \frac{\eta_m}{y}^x, X \equiv x \tag{9}$$

where η_m is a known function of M_ζ. Figure 8 indicates the flow and geometric parameters for the mixing region. The dividing streamline is defined as the limiting streamline capable of isentropic recompression to the freestream pressure p_∞. All flow in the mixing layer below this streamline is diverted into the dead-air region. Employing continuity, it may be shown that the base bleed flow rate G_B necessary to balance the fluid entrained across the dividing streamline is given by

$$G_B = \left[I_1(C_\zeta;\eta_s) - I_1(C_\zeta;\eta_j)\right]\frac{\rho_\zeta u_\zeta}{\sigma}(1-C_\zeta^2)A_{DS} \tag{10}$$

Here C_ζ is the Crocco number[11] based on the free-streamline Mach number M_ζ, ρ_ζ is the local density, and A_{DS} is the surface area of the dividing streamline from $x=0$ to the oblique shock. The functions $I_1(C_\zeta;\eta)$ and $\eta_j = \eta_j(\Phi_j(C_\zeta))$ are known and given in Ref. 11.

Thus, the analysis of the mixing region yields a relationship between the base drag coefficient and the base bleed flow rate. A solvable set of equations leading to a unique base drag coefficient for a given set of geometric and flow constraints requires, in addition to the results of the mixing layer and inviscid analysis, a closure criterion. The closure criterion is based on the conservation of momentum of the base bleed flow. Assuming a uniform base bleed flow rate acting over the area $\pi(r_{DS}^2 - r_S^2)$, where r_{DS} is the radius to the dividing streamline at the shock and r_S is the sting radius where $r_S < r_{DS}$, Eq. (11) may be formulated

$$C_{DB} = \frac{1}{K_{DS}}\left[\frac{H A_{DS}/A_B}{M_\infty(r_{DS}^2 - r_S^2)}\right]^2\left(\frac{\rho_\zeta}{\rho}\right)^2 \tag{11}$$

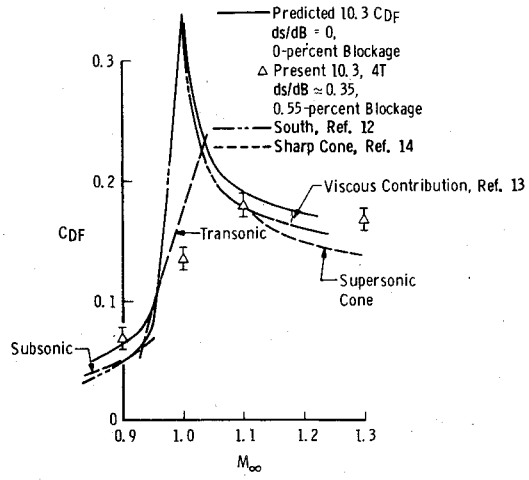

Fig. 9 Theoretical forebody drag coefficient for 10.3 cone.

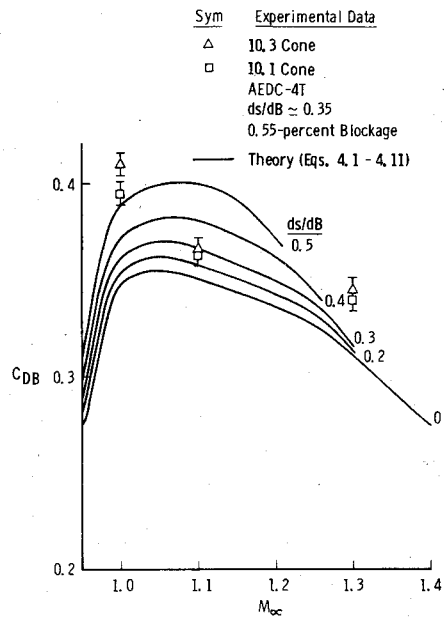

Fig. 10 Theoretical base drag coefficient for a 10 deg cone as a function of Mach number and sting to base diameter ratio.

with the bleed number H equal to $G_B/(\rho_\zeta a_\infty A_{DS})$ and a_∞ the freestream speed of sound. The coefficient K_{DS} is the fraction of energy the base bleed flow recovers in accelerating through the difference in base and freestream pressures and A_B is the cone base area. In general, K_{DS} is a function of the influence of the recompression region and the mixing layer on the ability of the base bleed to enter the dead-air region. Since, for the applications considered here, the effect of the mixing layer on the bleed flow will be approximately constant at the location of the oblique shock, it is assumed that the coefficient varies only with the dividing streamline angle at the shock location, giving $K_{DS} = K_{DS}(\zeta_{DS})$ (Fig. 8).

In order to evaluate the magnitude and variation of K_{DS} and ζ_{DS}, the free-flight characteristics of a 10.3 cone (Fig. 3), corrected for blockage interference, combined with theoretical predictions of the forebody drag C_{DF} (both wave[3] and viscous[13]) were used. Figure 9 is a graph of 10.3 cone forebody drag estimates including measured wind tunnel data. Also included for comparison is the wave drag contribution for sharp cones in the subsonic, transonic, and supersonic flow regions using the slender body theory of Sprieter.[14] The solid curve denoting C_{DF} was subtracted from the values of C_{D0} obtained by the extrapolation of the curves given in Fig. 4 to 0% blockage. The results gave a corrected base drag curve as a function of the freestream Mach number

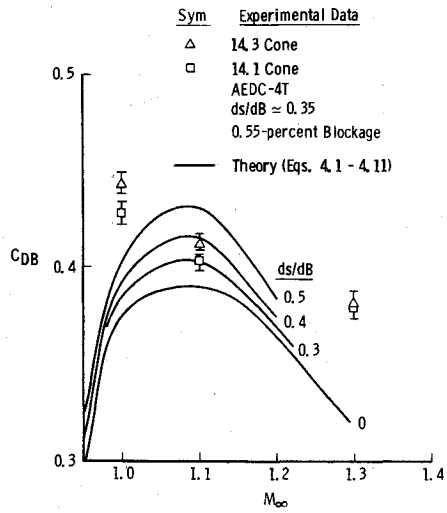

Fig. 11 Theoretical base drag coefficient for a 14 deg cone as a function of Mach number and sting to base diameter ratio.

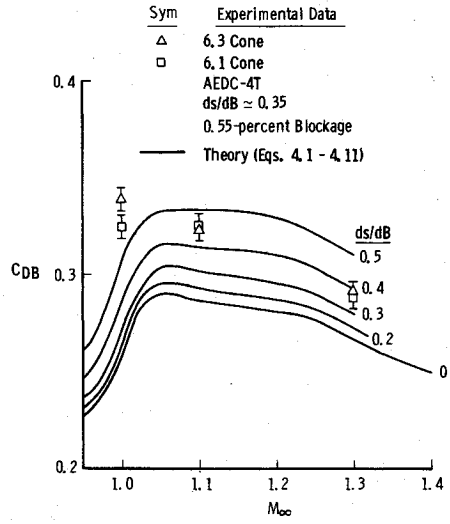

Fig. 12 Theoretical base drag coefficient for a 6 deg cone as a function of Mach number and sting to base diameter ratio.

M_∞ for no sting. The base drag curve in conjunction with the theory as given in Eqs. (1-11) was then used to evaluate the functional form of $K_{DS}(\zeta_{DS})$. Using the generated $K_{DS}(\zeta_{DS})$, the theoretical variation of the base drag coefficient for a 10 deg cone as a function of Mach number and the ratio of sting to base diameter, ds/dB, was evaluated and is shown in Fig. 10. Also included for comparison are data from the wind tunnel with 0.55% blockage and $ds/dB \simeq 0.35$. Considering the influence of blockage at or very near Mach 1 (see Fig. 9), the theoretical curve of C_{DB} vs M_∞ for $ds/dB \simeq 0.35$ appears to predict the order of magnitude and generally the correct trend of the sting correction when compared to the experimental data. The wind tunnel data presented in Figs. 10-12 at Mach 1.3 are felt to contain an unresolved bias when examined in lieu of available C_{DB} data at Mach 1.5.

Theoretical base pressure curves for cone angles of 6 and 14 deg were also established based on K_{DS} evaluated from the 10 deg data. These are given in Figs. 11 and 12. Agreement here between the theory and experiment is reasonable for Mach numbers outside of the region where blockage effects are important. By a comparison of the theoretical curves and data given in Figs. 10-12, the present theoretical model appears to give reasonable estimates of the effects of sting diameter, Mach number, and cone angle on base drag in the absence of wall interference.

A further check on the validity of the present flow model is afforded by the photographic data generated in the present

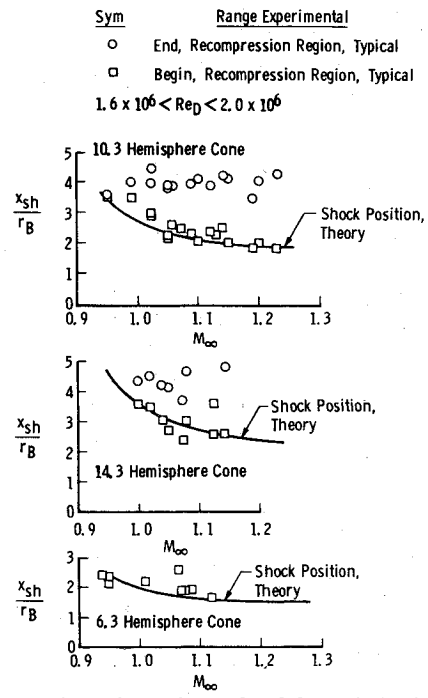

Fig. 13 Comparison of experimental and theoretical axial position of recompression region.

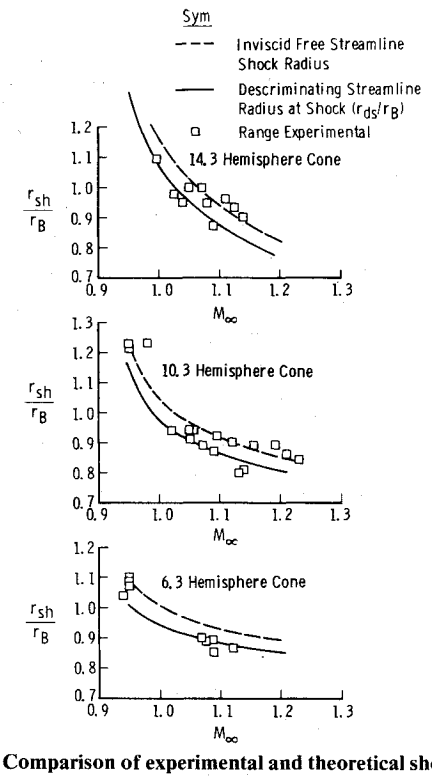

Fig. 14 Comparison of experimental and theoretical shock radius.

aeroballistic range test. Photographic data were reduced (with reference to Fig. 6) and the important wake geometric parameters are given in Figs. 13 and 14. Figure 13 is a comparison of the axial position of the experimental recompression region with the values predicted by theory. In spite of the fact that the theory assumed the recompression region to be an oblique shock, the model does give a reasonable estimate of the beginning of the recompression region for the range of cone angles and Mach numbers examined. The theoretical and experimental shock radius is compared in Fig. 14 and also shows good agreement both in trend and magnitude. With respect to the flow geometries considered,

the mixing layer is relatively thin as compared to the free-streamline radius and, thus, the experimental data taken can be used as a measure of the shock radius.

Referring to Figs. 10-12, for sting to base diameter ratios on the order of 0.3 or less, cone angle and Mach number for the range considered here have little effect on the drag coefficient relative to changes in ds/dB. This result is in agreement with the standard practice of simply shifting the C_{DB} curve by a constant amount to correct for sting effects across the entire Mach range considered. Thus, for $ds/dB \simeq 0.30$, the theory predicts a fractional increase in base drag of approximately 5%. As ds/dB is increased beyond 0.3, the base drag correction becomes highly nonlinear in both Mach number and cone angle. Within the range of the geometric flow variables considered, the present analysis may be applied to bodies of arbitrary forebody shape as long as the flowfield just upstream of the trailing edge is sonic or slightly greater and is approximately conical.

The preceding analysis has considered the effects of sting support, Mach number, and cone angle on the base drag characteristics of conical bodies. Certain assumptions were made in the course of the analysis. The compressive wave structure region as depicted in Fig. 6 was replaced by an oblique shock structure in the model. The asymmetry effects on the mixing-layer region were neglected and the influence of the finite boundary-layer thickness at the cone shoulder was not considered. Mueller[15] and others have suggested that all of the effects neglected here play an important role in defining the base drag coefficient for axisymmetric bodies. Comparisons presented here have shown, however, that reasonable agreement exists between the model proposed and available experimental results for variations in freestream Mach number, cone angle, and sting to base diameter.

Summary

In summary, a study to determine the actual drag variation on conical bodies at transonic speeds has yielded some additional insight into wall interference phenomena and sting effects. The effect of wall interference on the drag of these short conical bodies near Mach 1 is similar to those severe trends observed on longer slender bodies of revolution. The percentage reduction in drag at Mach 1 for increasing solid blockage is nearly identical for the two configurations. However, a transonic test section wall which can be reduced in porosity near Mach 1 relative to the correct setting at lower or higher Mach numbers (variable porosity with Mach number) appears to measurably reduce the wall interference problem.

The influence of a sting on the base drag of these bodies has been demonstrated to be important, altering the drag by as much as 5-10%, and a mathematical model of the base flowfield has been developed. This theoretical model treats the base drag of blunt-based bodies of revolution for various forebody cone angles and is valid for stings up to one-half the body diameter in size. The theoretical predictions of the influence of a sting on the base drag of conical bodies at transonic speeds is in excellent agreement with the experimentally observed trends.

References

[1] Lo, C. F. and Carleton, W., "Transonic Scaling Effect on a Quasi Two-Dimensional C-141 Airfoil Model," Arnold Engineering Development Center, Arnold Air Force Station, Tenn., AEDC-TR-73-61 (AD762285), 1973.

[2] Binion, T. W., "An Investigation of Three-Dimensional Wall Interference in a Variable Porosity Transonic Wind Tunnel," Arnold Engineering Development Center, Arnold Air Force Station, Tenn., AEDC-TR-74-76 (AD787658), Oct. 1974.

[3] Couch, L. M. and Brooks, C. W., "Effect of Blockage Ratio on Drag and Pressure Distributions for Bodies of Revolution at Transonic Speeds," NASA-TND-7731, Langley Research Center, Hampton, Va., Nov. 1973.

[4] Starr, R. F. and Schueler, C. J., "Experimental Studies of a Ludweig Tube High Reynolds Number Transonic Tunnel," Arnold Engineering Development Center, Arnold Air Force Station, Tenn., AEDC-TR-73-168 (AD771646), 1973.

[5] Jacocks, J. L., "Determination of Optimum Operating Parameters for the AEDC-PWT 4-ft Transonic Tunnel with Variable Porosity Test Section Walls, Arnold Engineering Development Center, Arnold Air Force Station, Tenn., AEDC-TR-69-164 (AD857045), Aug. 1969.

[6] Sidney, R., "Review of Base Drag," BRL R 1337, Oct. 1966.

[7] Tani, T., "Local Two-Dimensional Approximation for Axisymmetric Transonic Flow," *Japan National Congress for Applied Mechanics, 16th Proceedings*, 1967, pp. 224-228.

[8] Aoyama, K., "Analysis of Transonic Flow Field Around Bodies of Revolution," PhD. Dissertation, University of Tennessee, Knoxville, Tenn., June 1971.

[9] Korst, H. H., Page, R. H., and Childs, M. E., "A Theory for Base Pressures in Transonic and Supersonic Flow," University of Illinois ME Technical Note 392-2, March 1955; also *Journal of Applied Mechanics*, Vol. 23, Dec. 1956, pp. 593-600.

[10] Vasiliu, J., "Pressure Distribution in Regions of Step Induced Turbulent Separation," *Journal of Aerospace Sciences*, Vol. 29, May 1962, pp. 596-601, 631.

[11] Korst, H. H., Page, R. H., and Childs, M. E., "Compressible Two-Dimensional Jet Mixing at Constant Pressure," University of Illinois, Champaign-Urbana, Ill., Technical Note 392-3, April 1955.

[12] South, J. C. and Jameson, A., "Relaxation Solutions for Inviscid Axisymmetric Transonic Flow over Blunt or Pointed Bodies," *Proceedings of the AIAA Computational Fluid Dynamics Conference*, Palm Springs, Calif., July 19-20, 1973, pp. 8-17.

[13] Van Driest, E. R., "Turbulent Boundary Layer on a Cone in a Supersonic Flow at Zero Angle of Attack," *Journal of the Aeronautical Sciences*, Vol. 19, Jan. 1952, pp. 55-57, 72.

[14] Sprieter, J. R. and Alksne, A., Y., "Slender-Body Theory Based on Approximate Solution of the Transonic Flow Equation," NASA Technical Report R-2, 1959.

[15] Mueller, T. J., "Determination of the Turbulent Base Pressure in Supersonic Axisymmetric Flow," *Journal of Spacecraft and Rockets*, Vol. 5, Jan. 1968, pp. 101-107.